Supplemental Material for "Incoherent qubit control using the quantum Zeno effect"

S. Hacohen-Gourgy[1,2], L. P. García-Pintos[3,4], L. S. Martin[1,2], J. Dressel[3,4], and I. Siddiqi[1,2]

[1] *Quantum Nanoelectronics Laboratory, Department of Physics,*
University of California, Berkeley CA 94720, USA
[2] *Center for Quantum Coherent Science, Department of Physics,*
University of California, Berkeley CA 94720, USA
[3] *Institute for Quantum Studies, Chapman University, Orange, CA 92866, USA*
[4] *Schmid College of Science and Technology, Chapman University, Orange, CA 92866, USA*

TRAJECTORY RECONSTRUCTION

The stochastic master equation given in the main text is generated by the following measurement operator

$$\Omega(V) = \exp\left[-\frac{\Gamma_D \eta}{2}\left(V(t) - \sigma_{\delta(t)}\right)^2 dt\right] \tag{1}$$

$$\rho(t+dt) = \mathcal{E}_{1-\eta}\frac{\Omega\rho(t)\Omega^\dagger}{\mathrm{Tr}[\Omega\rho(t)\Omega^\dagger]},$$

where $\mathcal{E}_{1-\eta_i}$ is a superoperator which models dephasing due to finite quantum efficiency and small additional dephasing taken from the finite measured Rabi time. To ensure positivity of the state when dt is taken to be finite, we use Eq. (1) to numerically propagate the quantum trajectories. The parameters Γ_D and η are calibrated independently. The former we measure by preparing $|+\rangle$ and then performing a Ramsey measurement. We measure the quantum efficiency by preparing states $|y = \pm 1\rangle$. Histograms of the integrated measurement records yield a pair of Gaussians which separate as a function of time. The quantum efficiency is given by

$$\eta = \frac{(\mu_{y=+1} - \mu_{y=-1})^2}{8\tau\sigma^2\Gamma_D}, \tag{2}$$

where $\mu_{y=\pm 1}$ is the mean of the Gaussian for the $|y = \pm 1\rangle$ state preparation, σ is the average standard deviation of the Gaussians and τ is the measurement duration [1, 2].

When reconstructing the quantum trajectories and comparing the average of the trajectories to the solution for the the master equation for the the average state we found a disagreement between theory and experiment. This seemed to be a systematic discrepancy due to a small offset in the detector voltage. We corrected this using an informed 'guess' offset, which was calibrated from a different experiment [3] performed using the same setup. The offset value used is 0.17V where the separation of the mean of the Gaussians for this detector was 1.74V. In Fig. 1 we show the comparison of the average of the trajectories with theory for 3 dragging velocities, for processing with and without the correction. In the main text we use the corrected data.
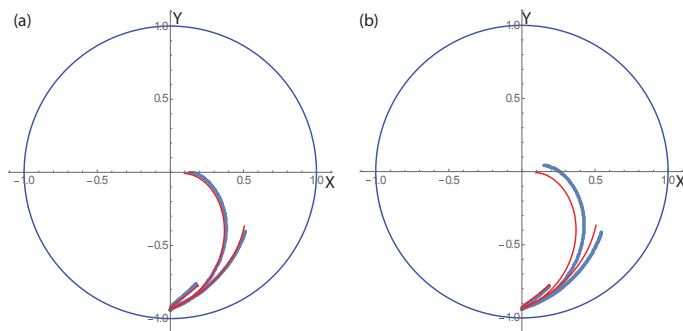

FIG. 1: Average of the experimental trajectories before (b) and after (a) correction of offset in detector voltage, compared to theory for 3 example dragging velocities of 0.01 MHz, 0.04 MHz and 0.1 MHz. Blue is the average of the experimental trajectories and the red line is the solution to the master equation.

DEVICE PARAMETERS

The transmon qubit is fabricated on double-side-polished silicon, with a single double-angle-evaporated Al/AlOx/Al Josephson junction. The internal dimensions of the aluminum 3D cavity are 81 mm x 20 mm x 5 mm. The qubit is positioned 23 mm from the edge of the cavity. The qubit has a transition frequency of $\omega_q/2\pi$ = 4.262 GHz, an energy-decay timescale of T_1 = 60 μs, and a dephasing timescale of T_2^* = 30 μs. For this experiment we use the second lowest cavity mode, with a frequency of $\omega/2\pi$ = 7.391 GHz, and a linewidth of $\kappa/2\pi$ = 4.3 MHz. The qubit dispersive frequency shift is $\chi/2\pi$ = -0.23 MHz.

The qubit pulses and the sidebands are generated by using single sideband and double sideband modulation respectively. For the qubit, this makes the tomography pulses simpler. The phase of the modulation is set by the arbitrary waveform generator (ARB), hence the tomography pulses along the different axes amount to simply changing the modulation phase. For the sidebands, using double sideband modulation is the key to dynamically varying the sideband phase difference, and hence varying the measurement operator. In practice this amounts to a small frequency detuning, for example for a measurement operator rotating at $v = 0.01$ MHz we set the sideband modulation frequency to 40.01 MHz = 40.00 MHz + 0.01 MHz.
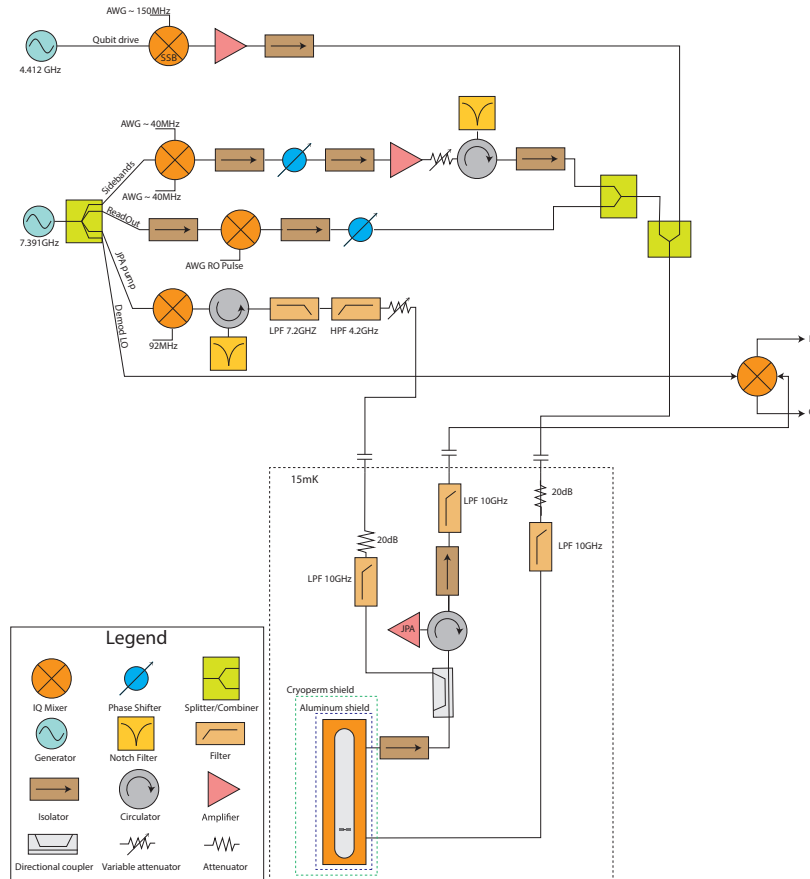

FIG. 2: Schematic illustration of the experimental setup - We use one generator detuned above the qubit frequency by 150MHz, and a single sideband modulator, controlled by the AWG to generate qubit pulses. Due to the high Rabi frequency of 40 MHz we require a following amplifier. We use a second generator set to the frequency of the cavity, the power is split 4 ways. One is mixed using an IQ mixer to generate the sidebands. These are controlled by the AWG. the following phase shifter is used to align the readout quadrature to the one amplified by the JPA. The LO leakage tone is then filtered using a home built notch filter. Second is used for doing a strong dispersive readout of the bare qubit, the following phase shifter is used to align the dispersive readout phase to the JPA phase. Third split is used again for double sideband modulation and is sent to the JPA to pump it for gain. Fourth split is used as the LO reference of demodulating the output signal. Inside the dotted line is the cryogenic setup at base temperature. The cavity has a weakly coupled port for input, and a strongly coupled port for output. The JPA pump is coupled using a directional coupler.

STATISTICS OF POSTSELECTION

Fig. 4 in the main text shows the average fidelity as function of postselection threshold for 6 dragging velocities. Here we show detailed statistics for one of the dragging velocities $v = 0.06$ MHz, other velocities show similar features. In the experiment we had $\sim 20,000$ traces for each velocity. The number of traces varies by a few percent from velocity to velocity due to Heralding. We have also simulated the experiment with 20,000 traces and with 200,000 traces in order to compare to the data. In Fig.3b we can see the average fidelity for the data and the simulations for $v = 0.06$ MHz. The histogram, and the simulation data show that the fidelity for the most negative postselections drops due to rare fluctuations that average away in the signal, but still have a residual effect on the state evolution. On Fig. 4 we show the statistics of how many trajectories passed each threshold, this shows that very high fidelity occurs for only a fraction of a percent of the events.
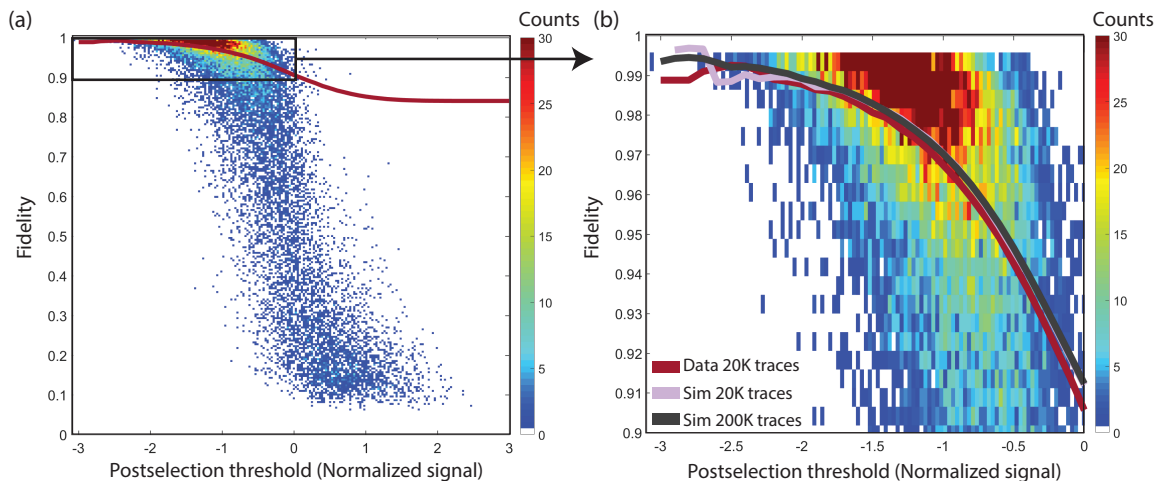

FIG. 3: Statistics of the postselection for dragging velocity of 0.06 MHz. The colorplot histogram shows how many trajectories reached a certain fidelity for each postselection threshold. The lines are the average fidelity as function of postselection for the data and simulations. Since the data and simulation are very similar, for clarity in (a) we only plot the data and in (b) we overlay the data and simulation results and zoom in on the relevant region.
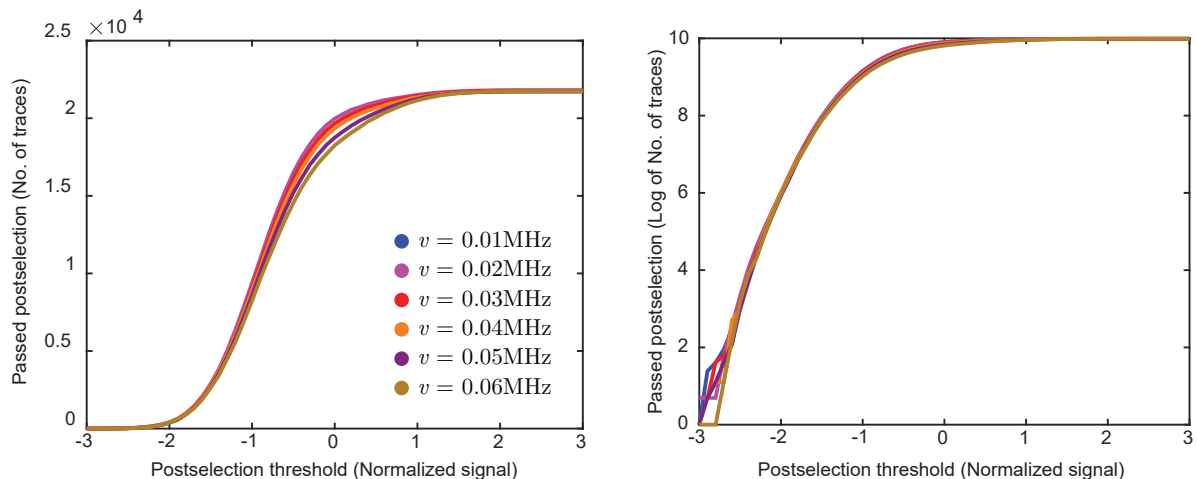

FIG. 4: Statistics of the postselection, showing how many trajectories passed each threshold for the same dragging velocities as shown in Fig.4 of the main text. Linear scale is shown in (a), log scale is shown in (b).

DETAILS OF JUMP AXIS DERIVATION

For our specific experiment the ensemble averaged dynamics can be solved analytically by going into a frame rotating at the dragging velocity v, where the measurement axis is fixed and the qubit is driven by the Hamiltonian $H = (\Omega/2)\sigma_z$, with $\Omega = 2\pi v$. In this measurement-axis frame the average qubit state evolves according to

$$\dot{\rho} = -i\frac{\Omega}{2}[\sigma_z, \rho] - \Gamma\frac{\left[[\rho, \sigma_y], \sigma_y\right]}{4} + \frac{\xi_y}{\sqrt{\tau}}\left[\frac{\{\sigma_y, \rho\}}{2} - \mathrm{Tr}\left[\rho\sigma_y\right]\rho\right], \tag{3}$$

where the measurement axis is now fixed along the y direction, and for simplicity we drop the negligible pure dephasing term Γ_ϕ. Assuming an initial state confined to the $z = 0$ plane on the Bloch sphere, and using the fact that equation (3) does not take the qubit out of this plane, the ensemble-averaged equations of motion for the qubit components $x_m = \mathrm{Tr}\left[\rho\sigma_x\right]$ and $y_m = \mathrm{Tr}\left[\rho\sigma_y\right]$ are,

$$\dot{x}_m = -\Gamma_D x_m + \Omega y_m \tag{4}$$
$$\dot{y}_m = -\Omega x_m, \tag{5}$$

The eigenvectors are,

$$\vec{V}_\pm = \left(1, \frac{\lambda_\pm + \Gamma_D}{\Omega}\right) \tag{6}$$

and the eigenvalues are,

$$\lambda_\pm = \frac{-\Gamma_D \pm \sqrt{\Gamma_D^2 - 4\Omega^2}}{2}. \tag{7}$$

The evolution of the system on the measurement frame is then given by the vector $\vec{W}(t)$:

$$\vec{W}(t) = ae^{\lambda_+ t - \Gamma_C t}\vec{V}_+ + be^{\lambda_- t - \Gamma_C t}\vec{V}_-, \tag{8}$$

where the constants a and b are determined by the initial conditions.

---

[1] A. N. Korotkov, in *Quantum machines, Lecture notes of the Les Houches Summer School (Session 96, July 2011)*, edited by M. Devoret et al. (Oxford University Press, Oxford, 2014), p. 533, arXiv:1111.4016.
[2] A. N. Korotkov, Phys. Rev. A **94**, 042326 (2016).
[3] J. Atalaya, S. Hacohen-Gourgy, L. S. Martin, I. Siddiqi, and A. N. Korotkov, arXiv preprint arXiv:1702.08077 (2017).